A COMPREHENSIVE PERFORMANCE COMPARISON OF RFI MITIGATION TECHNIQUES FOR UWB RADAR SIGNALS

Lam H. Nguyen[1] and Trac D. Tran[2]
[1]U.S. Army Research Laboratory, Adelphi, MD 20783. Email: lam.h.nguyen2.civ@mail.mil
[2]Johns Hopkins University, Baltimore, MD 21218. Email: trac@jhu.edu

ABSTRACT

This paper presents a comprehensive benchmark comparison in objective as well as subjective performances of radio-frequency interference (RFI) suppression/extraction techniques for ultra-wideband (UWB) signals in synthetic aperture radar (SAR) imaging applications. In this study, we employ two sets of UWB SAR signals: one simulated from a step-frequency radar setup, whereas the other is collected on the testing field in a real-world setup from the U.S. Army Research Laboratory. Similarly, our RFI experiments involve two RFI data sets: one is simulated from a collection of randomly generated frequency bands and the other is the RFI data collected in a real-world environment with the radar receiving antenna pointing toward Washington DC. These SAR and RFI data sets represent four diverse experimental setups where we can carefully benchmark the denoising performance of several popular RFI-mitigation techniques in the current literature based on notch-filtering, principal component analysis (PCA), model-based sparse recovery, and simultaneous low-rank and sparse recovery or robust PCA (RPCA). We validate that RPCA and model-based sparse recovery consistently yields the best overall RFI separation performance on a wide range of settings in all data sets.

Index Terms — noise-source separation, radio-frequency interference, RFI, ultra-wideband, SAR

1. INTRODUCTION

Ultra-wideband (UWB) radars – transmitting signals in a wide frequency spectrum from under 100 MHz to several GHz – provide high imaging resolution and valuable penetrating power. These systems are very popular in numerous military and surveillance applications such as foliage-penetration (FOPEN), sensing-through-the-wall (STTW), and automatic detection of improvised explosive devices (IED) [1]-[4]. Unfortunately, UWB receivers are susceptible to corruptive radio-frequency interference (RFI) sources since the radar operating spectrum in this case is often dominated by various signal modulation schemes popular in wireless broadcasting and communication, resulting in a severely reduced signal-to-noise ratio (SNR), and hence, the final synthetic aperture radar (SAR) image quality. Mitigation of RFI is a critical challenge for UWB radars. Unfortunately, this is a notoriously difficult problem due to the dynamic and unpredictable nature of the noise sources, not to mention the strength of the noisy signals. Previous work in this RFI-mitigation area can be classified into two categories: *(i)* ***RFI suppression*** via filtering techniques, where estimated RFI sources are filtered out or suppressed under the noise floor; and *(ii)* ***RFI extraction***, where RFI components are first identified, estimated, and then subtracted out of the observed signals. Following the former approach include notch filtering, sub-band filtering, and/or adaptive filtering techniques, which are popular in practical implementations due to their simplicity [5]-[6]. The latter extraction approach comprises techniques employing parametric noise modeling [6], independent component analysis [7], eigensubspace decompositions [8]-[9], and sparse recovery [10]-[12].

In many research areas, e.g., computer vision, machine learning and compression, there exist diverse, well-designed standard data sets along with corresponding benchmarking mechanisms for researchers to compare different proposed approaches. Such public-domain data sets are rare in radar imaging – all of these aforementioned previous works present results on different data sets with very different assumptions, making performance comparison extremely difficult. In this paper, we try to take the first step in addressing this issue. Our main contributions include *(i)* we carefully design several diverse data set with realistic SAR signals and RFI sources via combination of both simulation and real data collected from well-controlled, real-world environments; *(ii)* we present a comprehensive comparison of popular RFI-mitigation techniques on these same data set; *(iii)* we show that robust principal component analysis (RPCA) and the model-based sparse recovery offers the most effective tool to tackle this RFI mitigation problem for UWB radars; and *(iv)* we intend to make these data sets available to all researchers in the field for algorithm testing and evaluation.

2. BACKGROUND: UWB SAR AND RFI MODELING

Let us consider a simplistic impulse-based SAR system trying to capture a simple scene with only two

significant targets, as depicted in Fig. 1. At aperture *i*, the transmitter would transmit a probing pulse ***s*** and the receiver would record the echoed backscattered signal $\mathbf{x}_i$. In the ideal case with exactly two point targets and without any interference, we expect the received signal to contain two backscattered pulses indicating how far apart our targets are with respect to the sensing platform. Note that this example illustrates precisely a UWB radar system, since the impulse in time leads to a wideband frequency representation.

In practice, UWB radar signals are often susceptible to interference by wireless signals $\mathbf{r}_i$ from AM/FM radios, TV broadcasting, mobile phone communications, etc. Hence, at each aperture, we instead observe $\mathbf{y}_i=\mathbf{x}_i+\mathbf{r}_i$ with the following common characteristic: narrow pulses $\mathbf{x}_i$ indicating the presence of significant targets of interest embedded in a sea of RFI waves $\mathbf{y}_i$. In short, SAR signals $\mathbf{x}_i$ are sparse in the time domain (wideband), whereas RFI signals $\mathbf{r}_i$ are sparse (narrowband) in the frequency domain. They come from completely independent sources and they behave very different statistically. This critical property makes signal-interference separation possible when we observe the mixture $\mathbf{y}_i$. In other radar implementations such as chirp or stepped-frequency, an extra signal pre-processing step is necessary to fit the observed data to this model. When data from all apertures are grouped together column-wise, we have the matrix model $\mathbf{Y} = \mathbf{X}+\mathbf{R}$.

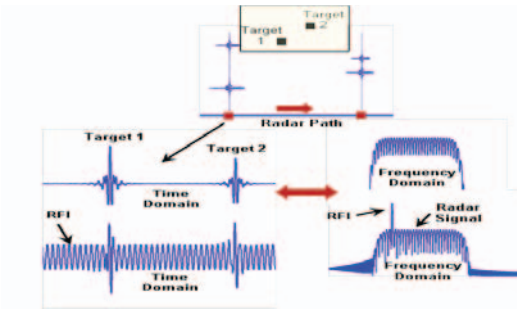

Figure 1. A simple illustration of an impulse-based UWB SAR received signals, with and without RFI.

3. BENCHMARKING DATA SETS AND RFI MITIGATION APPROACHES

Our experiments are conducted on an UWB step-frequency simulated data set as well as on a real impulse-based UWB BoomSAR data set collected from the U.S. Army Research Laboratory (ARL) radar [3]. Our simulated SAR data set is generated from a monostatic, side-looking, step-frequency SAR model setting with 1200 aperture positions in a straight line, imaging a scene with around 30 point targets of various amplitudes located in a uniform rectangular array. The largest targets are calibrated at the amplitudes of 0 dB, and the smallest targets have the amplitudes of –35 dB. The SAR signals occupy a spectrum from 300 to 1500 MHz, with no energy outside this band. However, since the energy is tapered at both ends of the spectrum, the effective spectrum of the SAR data spans approximately from 350 to 1450 MHz.

The real UWB low-frequency BoomSAR data set is collected from ARL UWB low-frequency SAR that transmits impulse radar signals that generate instantaneously a wide bandwidth that spans approximately 50 to 1150 MHz. The UWB BoomSAR is mounted on a platform that emulates the airborne geometry [3].

There are also two different RFI noise data sets in our experiments: the simulated RFI data set is generated from randomly modulated tones, whereas the real RFI data set is collected from the real environment with the antenna pointing toward Washington, D.C. In the real RFI case, for each aperture location *i* where radar data are collected, a segment of noise record is randomly captured and added to the raw radar data record. In this case, we cannot control the RFI bandwidth level. Hence, we have to employ a simple scaling factor to control the interference power level.

Our simulated RFI data set presents a more challenging scenario. At each aperture position, the RFI signal is simulated by generating many individual RFI sources (or bands). Each RFI source is a modulated signal with a bandwidth of 6 MHz, composed of many tones within its bandwidth. Each tone has a uniformly distributed random amplitude and phase. Thus, the analog model for such RFI signal at each aperture record is

$$r(t)=\sum_{j=1}^{M}\sum_{i=1}^{N}A_{ij}\cos\left(2\pi\left(f_j+\Delta fi\right)t+\theta_{ij}\right)$$

where M is the total number of RFI sources across the SAR spectrum, N is the number of tones within each RFI source, A_{ij} is the amplitude of each tone and is uniformly distributed within the interval $[0,\ A]$, f_j is the start frequency of the *jth* RFI source, Δf is the frequency spacing between the tones that compose an RFI source, and θ_{ij} is the phase of each tone, again uniformly distributed within the interval $[0, 2\pi]$.

RFI signals generated with its contents within its bandwidth are completely random. It represents a more challenging noise source compared to other practical modulation schemes such as AM, FM, and/or other digital modulation sources. Given the RFI to SAR bandwidth ratio, a number of 6-MHz RFI sources are generated across the SAR spectrum. It is likely that some of them are adjacent to others, forming RFI sources with bandwidths larger than 6 MHz. In addition, even with an individual RFI source of 6 MHz, the width of its main lobe overlaps a much larger bandwidth with the SAR data. Again, these simulated RFI signals are selected at random and added to the original SAR data to simulate RFI-contaminated signals. In the simulated RFI case, we do have control of both RFI bandwidth as well as RFI power level.

To benchmark RFI suppression/extraction performance, we propose to employ the root-mean-square (RMS) error as well as the SNR between the original data records and the recovered ones either directly in the time domain or between the original SAR image and the image from recovered signals:

$$RMS(\mathbf{x}) = \frac{1}{\sqrt{N}}\|\mathbf{x}\|_2 ; \qquad SNR(\mathbf{x},\hat{\mathbf{x}}) = 20\log_{10}\frac{RMS(\mathbf{x})}{RMS(\hat{\mathbf{x}}-\mathbf{x})}$$

We also define the processing gain (PG) as follows:

$$PG = 20\log_{10}\frac{RMS(\mathbf{x})}{RMS(\hat{\mathbf{x}}-\mathbf{x})} - 20\log_{10}\frac{RMS(\mathbf{x})}{RMS(\mathbf{y}-\mathbf{x})}$$

where $\mathbf{x}$ is the original SAR signal/image, $\hat{\mathbf{x}}$ is the recovered SAR signal/image, and $\mathbf{y}$ is the observed RFI-contaminated signal/image.

With two SAR and two RFI data sets, we can generate a total of four different testing scenarios: *(i)* simulated SAR with simulated RFI signals, *(ii)* simulated SAR with real RFI signals, *(iii)* real SAR with simulated RFI signals, and finally *(iv)* real SAR with real RFI signals. Since RFI are artificially injected into the SAR signals, ground truths are available for all testing scenarios, allowing us to compute many objective performance measures mentioned above.

4. ALGORITHMS IN COMPARISON

We select the following four RFI-mitigation techniques for performance comparison in this study.

Notch Filtering [5]-[6] [11]. We employ a simple spectrum estimator based on averaging of observed signals $\mathbf{Y}$ as described in [11] to identify RFI-dominant sub-bands and then suppress these RFI peaks with narrowband filters. This classical technique is simplest, fastest, and often the first choice in practical systems. However, notching is known to adversely affect the strength of SAR signals and introduce significant sidelobes, leading to severe ringing problems in the final SAR image.

Eigensubspace Decomposition or PCA [7]-[9]. At each aperture, the observed data matrix $\mathbf{Y}$ is constructed from segments of the received signal $\mathbf{y}_i$. RFI components are then estimated from dominant eigenvalues and RFI is extracted out of the observed $\mathbf{Y}$ via subspace projection. The main problem here is that PCA has no discriminative power and it only works well when RFI has really narrow bandwidth and its energy is significantly higher than that of SAR signals.

Sparse Recovery [10]-[12]. This approach constructs the SAR dictionary $\mathbf{D}^x$ from the transmitted waveforms and an estimated RFI dictionary $\mathbf{D}_i^r$ from the observed signals; we then solve the optimization problem (with orthogonal matching pursuit [OMP]):

$$\{\hat{\boldsymbol{\alpha}}_i, \hat{\mathbf{e}}_i\} = \underset{\boldsymbol{\alpha}_i, \boldsymbol{\varepsilon}_i}{\arg\min} \left\| \mathbf{y}_i - \mathbf{D}^x\boldsymbol{\alpha}_i - \mathbf{D}_i^r\mathbf{e}_i \right\|_2 \text{ s.t. } \|\boldsymbol{\alpha}_i\|_0 + \|\mathbf{e}_i\|_0 \le S$$

to extract out the RFI component $\hat{\mathbf{r}}_i = \mathbf{D}_i^r\hat{\mathbf{e}}_i$. Sparse recovery generally works well in all scenarios. Its main drawback comes from the additional step of dictionary learning. The next sections shows that, when the data model is accurate, sparse recovery yields the best performance.

RPCA [13]-[14]. The simultaneous low-rank and sparse recovery approach [13] models the problem via RPCA [14]. The RFI components $\mathbf{R}$ are modeled as low-rank whereas the SAR signals $\mathbf{X}$ are treated as spikey sparse outliers. RFI components can be extracted via solving:

$$\{\hat{\mathbf{R}}, \hat{\mathbf{X}}\} = \underset{\mathbf{R},\mathbf{X}}{\arg\min} \|\mathbf{R}\|_* + \lambda\|\mathbf{X}\|_1 \quad \text{s.t.} \quad \mathbf{Y} = \mathbf{X} + \mathbf{R}.$$

where $\|\mathbf{R}\|_*$ is the nuclear norm of $\mathbf{R}$ (approximating its rank) while $\|\mathbf{X}\|_1$ is the ℓ_1 entry norm of $\mathbf{X}$ (approximating its sparsity level). The competition between the rank of $\mathbf{R}$ and the sparsity of $\mathbf{X}$ encourages a clustering behavior, leading to the separation between SAR and RFI components. In all 4 data sets, RFI extraction can be achieved ***blindly*** without the need of any prior information!

5. EXPERIMENTAL RESULTS

This section presents the RFI mitigation performance of all four algorithms as mentioned in Section 4. Fig. 2 shows the results from the simulated radar data set that are injected with the simulated RFI data. The radar signal to RFI energy ratio in this case is –30 dB. Fig. 2a shows the spectral contents of the original data, RFI data, and RFI-contaminated radar data. Fig. 2b shows the SAR image of the simulation scene without noise. Fig. 2c shows the SAR image formed using the RF-contaminated radar data. Figure 2d-g shows the recovered SAR images using the notch filtering, the eigensubspace, the low-rank and sparse recovery, and the model-based sparse recovery techniques, respectively. The baseline notch filtering achieves a processing gain of 15.47 dB. The eigensubspace achieves a lowest performance among the algorithms, with only 3.02 dB of processing gain. The simultaneous low-rank and sparse recovery achieves an impressive processing gain of 24.42 dB. However, a few smallest targets in the scene are not discernable in the SAR of Fig. 2f. Finally, thanks to effective modeling, the model-based sparse recovery technique achieves a highest processing gain of 27.45 dB. All 30 targets in the SAR image of Fig. 2g are discernable.

Fig. 3 depicts the results using radar data from the ARL BoomSAR injected with measured RFI from the urban environment. The radar signal to RFI energy ratio in this case is also set at –30 dB. The results from this real data experiment also show that the low-rank and sparse recovery, and the model-based sparse recovery techniques achieve the highest processing gains of 19.43 and 18.0 dB, respectively. In this realistic scenario, modeling accuracy is inexact, and the blind RPCA approach turns out to be more effective.

Fig. 4 compares the RFI objective suppression performance in the SAR imagery (simulated data) domain using the four techniques over a large range of RFI

bandwidth setting, with the SAR to RFI signal ratio is fixed at –30 dB. The processing gain curves illustrated in Fig. 4 show that both the low-rank and sparse recovery, and the model-based sparse recovery exhibit a much higher level of robustness. Even with the very challenging case of RFI to SAR bandwidth ratio of 30%, they achieve a processing gain of approximately 15 dB.

Fig. 5 compares the RFI objective suppression performance of the four techniques in the SAR imagery domain using real radar data from the ARL BoomSAR and real RFI data with various settings of SAR to RFI signal ratio. Both the model-based sparse recovery and the RPCA techniques achieve good performance and outperform others over a wide range of SNR.

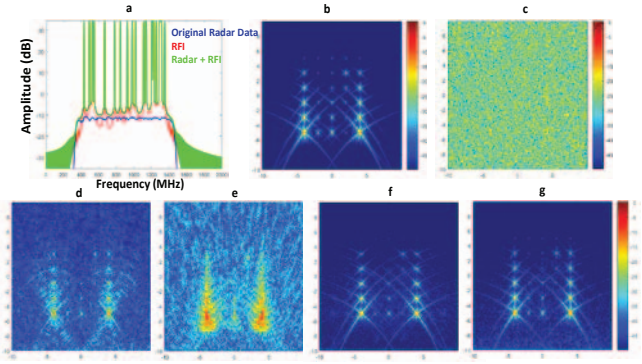

Figure 2. RFI suppression performance using simulation SAR and RFI data (SNR= –30 dB). (a) Spectrum of SAR, RFI, and SAR plus RFI signals. (b) Original SAR image. (c) SAR image with RFI noise; SNR = –13.47 dB (d) SAR image (notch filtering): processing gain = 15.47 dB; SNR = 2.0 dB. (e) SAR image (PCA): processing gain = 3.02 dB; SNR = –10.45 dB. (f) SAR image (RPCA): processing gain = 24.42 dB; SNR = 10.95 dB. (g) SAR image (model-based sparse recovery): processing gain = 27.45 dB; SNR = 13.98 dB.

6. CONCLUSION

This paper presents our first step in designing a standard SAR and RFI data set and the performance metrics for the evaluation of RFI suppression in low-frequency UWB radar applications. This framework allows us understand the strengths and limitations of various RFI mitigation algorithms, leading to the development of more robust solutions for the congested spectrum challenge, which is the most critical challenge for low-frequency UWB radar.

We also present the initial performance comparison (both subjectively and objectively) using four different RFI mitigation techniques with our common data sets: simulation and real data from ARL UWB SAR radar. An early observation in this evaluation process is that RPCA (where RFI makes up the low-rank components while SAR signals play the role of sparse outliers) with its additional discriminative power offers the best RFI suppression performance. Its performance is surprisingly comparable to that of model-based sparse recovery technique, which requires accurate prior information on the radar signals as well as RFI characteristics.

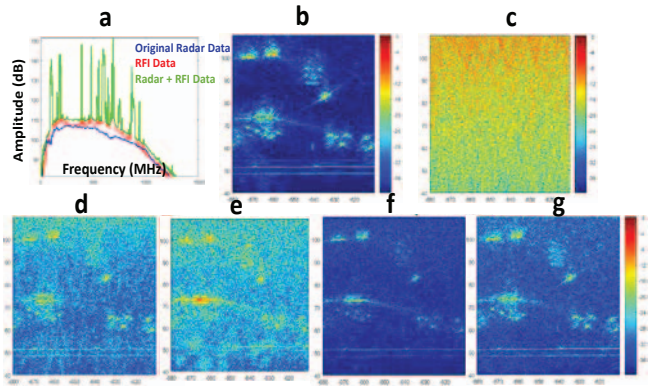

Figure 3. RFI suppression performance using data from the ARL BoomSAR radar and real RFI data (raw SNR= –30 dB). (a) Spectrum of SAR, RFI, and SAR plus RFI signals. (b) Original SAR image. (c) SAR image with RFI noise; SNR = 17.97 dB (d) SAR image (notch filtering): processing gain = 13.72 dB; SNR = –4.4 dB. (e) SAR image (PCA): processing gain = 9.9 dB; SNR = –8.1 dB. (f) SAR image (RPCA): processing gain = 20.3 dB; SNR = 2.35 dB. (g) SAR image (model-based sparse recovery): processing gain = 19.0 dB; SNR = 1.03 dB.

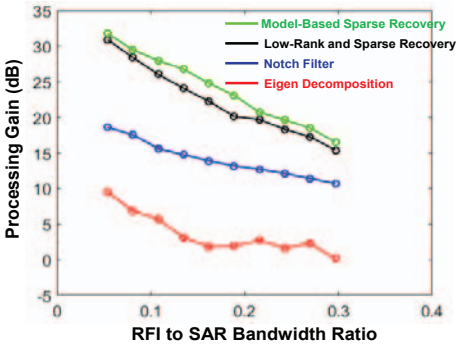

Figure 4. RFI objective suppression performance in the SAR imagery in the SAR imagery (simulated data) domain using the four techniques over a large range of RFI bandwidth settings.

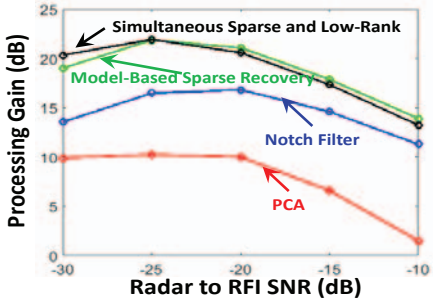

Figure 5. RFI objective suppression performance in the SAR imagery in the SAR imagery domain using real radar data from the ARL BoomSAR and real RFI data with various settings of SAR to RFI signal ratio.

7. REFERENCES

[1] J. D. Taylor, ed. *Ultra-wideband Radar Technology*, CRC press, 2000.

[2] S.-E. Hamran. *Radar Performance of Ultra-wideband Waveforms*. INTECH Open Access Publisher, 2010.

[3] M. A. Ressler, "The Army Research Laboratory Ultra Wideband BoomSAR," *IEEE IGARSS*, pp. 1886-1888, 1996.

[4] M. Davis, "Frequency allocation challenges for ultra-wideband radars," *IEEE Aerosp. Electron. Syst. Mag*., vol. 28, no. 7, pp. 12–18, Jul. 2013.

[5] T. Koutsoudis and L. A. Lovas, "RF interference suppression in ultra-wideband radar receivers," *Proc. of the SPIE, Int. Symp. on Alg. for SAR Imagery II*, vol. 2487, pp. 107-118, Apr. 1995.

[6] T. R. Miller, J. McCorkle, and L. C. Potter, "Radio frequency interference suppression for foliage penetrating radar imaging," *IEEE Trans. on AES*, vol. 33, pp. 1142—1156, Oct. 1997.

[7] F. Zhou, M. Tao, and X. Bai, "Narrow-band interference suppression for SAR based on independent component analysis," *IEEE Trans. on Geo. and Remote Sensing*, vol. 51, pp. 4952-4960, Oct. 2013.

[8] F. Zhou, R. Wu, M. Xing, and Z. Bao, "Eigensubspace-based filtering with application in narrow-band interference suppression for SAR," *IEEE Geo. and Rem. Sen. Let.*, vol. 4, pp. 75-79, 2007.

[9] F. Zhou and M. Tao, "Research on methods for narrow-band interference suppression in synthetic aperture radar data," *IEEE JSTARS*, vol. 8, no. 7, pp. 3476-3485, July 2015.

[10] L. H. Nguyen, T. D. Tran, and T. Do, "Sparse models and sparse recovery for ultra-wideband SAR applications," *IEEE Trans. on AES,* vol. 50, no. 2, pp. 940-958, 2014.

[11] L. H. Nguyen and T. D. Tran, "Estimation and extraction of radio-frequency interference from ultra-wideband radar signals," *IEEE IGARSS*, pp. 2848-2851, Jul. 2015.

[12] L. H. Nguyen and T. D. Tran, "Efficient and robust RFI extraction via sparse recovery," *IEEE J. Sel. Topics in Applied Earth Obs. and Remote Sensing*, vol. 9, pp. 2104-2117, 2016.

[13] L. H. Nguyen and T. D. Tran, "RFI-Radar signal separation via simultaneous low-rank and sparse recovery," *IEEE Radar Conference*, May 2016.

[14] E. J. Candès, X. Li, Y. Ma, and J. Wright, "Robust principal component analysis?" *Journal of ACM*, vol. 58, pp. 1-37, 2009.